

Onset of multifragment emission in heavy-ion collisions

R. Trockel, K. D. Hildenbrand, U. Lynen, W. F. J. Müller,* H. J. Rabe,
H. Sann, H. Stelzer, W. Trautmann, and R. Wada†

Gesellschaft für Schwerionenforschung Darmstadt m.b.H., D-6100 Darmstadt, West Germany

E. Eckert, P. Kreuzt, A. Kühmichel, and J. Pochodzalla
Universität Frankfurt, D-6000 Frankfurt, West Germany

D. Pelte

Universität Heidelberg, D-6900 Heidelberg, West Germany

(Received 17 May 1988; revised manuscript received 12 October 1988)

A multidetector setup with large solid angle coverage has been used to measure the particle and fragment emission associated with the production of intermediate mass fragments in reactions of ^{12}C , ^{18}O , ^{20}Ne , and ^{40}Ar on $^{\text{nat}}\text{Ag}$ and ^{197}Au at bombarding energies $30 \text{ MeV} \leq E/A \leq 84 \text{ MeV}$. It is found that the cross sections, the element distributions, and the multiplicities of intermediate mass fragments are strongly correlated with the excitation energy E_x deposited in the composite system and that multifragment emission sets in at $E_x \cong 300 \text{ MeV}$.

Multifragmentation is predicted to be a dominant decay mode of highly excited heavy nuclei,^{1,2} and multifragment processes, i.e., reactions producing several complex nuclear fragments, have indeed been observed experimentally, first in emulsion data many years ago³⁻⁵ and, more recently, in electronic counter experiments.⁶⁻⁹ At present it is not clear, however, whether these multifragment events result from a qualitatively new reaction mode pertinent to the regime of high-energy heavy-ion reactions or rather from a sequence of more conventional fission-like processes. The answer must come both from specific experiments sensitive to the time scales¹⁰ and the breakup configurations in these processes as well as from systematic studies over a wide range of reactions and bombarding energies which are capable of identifying the conditions leading to multifragment decay. Here we report the results of a first survey of the latter kind. It includes ten different reactions which, as it turns out, cover the threshold region where multifragment emission starts to appear as a major mode of nuclear disintegration. As a main result, it is found that the excitation energy residing in the composite system before fragment emission is the key variable governing these processes.

Beams from the CERN synchrocyclotron (^{12}C of $E/A = 30, 48, \text{ and } 84 \text{ MeV}$; ^{18}O of $E/A = 84 \text{ MeV}$; and ^{20}Ne of $E/A = 48 \text{ MeV}$) and from the SARA facility in Grenoble (^{40}Ar of $E/A = 30 \text{ MeV}$) were used to bombard $^{\text{nat}}\text{Ag}$ and ^{197}Au targets of areal densities between 0.5 and 3.0 mg/cm². The multidetector setup covering a major fraction of the 4π solid angle was designed to simultaneously detect and identify light particles and nuclear fragments. It consisted of (i) an array of five detector telescopes¹¹ with solid angles of up to $\Delta\Omega = 3.9 \text{ msr}$ sampling the range of laboratory angles between 29° and 119° , (ii) an array of twelve large area parallel plate avalanche counters (PPAC's), which covered $\Delta\Omega = 2.7\pi \text{ sr}$ between $\Theta = 22^\circ$ and $\Theta = 158^\circ$, that were backed by an array of ten plastic scintillators of 1 cm thickness and $\Delta\Omega = 1.8\pi \text{ sr}$, and (iii) a forward hodoscope of 54 plastic and

phoswich detectors extending over the angular range $2.5^\circ \leq \Theta \leq 20^\circ$.¹²

The telescopes served as the trigger detectors. Coincident intermediate mass fragments (IMF's, here defined as nuclear fragments with an atomic number $3 \leq Z \leq 20$) were detected with the PPAC array and distinguished from the heavier fission fragments and heavy recoil nuclei by their different pulse height and time of flight. (The time zero of the reaction was reconstructed from the measured energies and times of the trigger particles and fragments.) This was verified for those fragments that were identified with the telescopes after having passed the PPAC's in front of them. The efficiency of the PPAC's to detect impinging fragments, determined in the same way, was found to be $\cong 80\%$ for boron and essentially 100% for carbon and heavier ions.¹³ The overall efficiency of the array of PPAC's to detect IMF's of $Z \geq 3$ was about 50% and nearly the same for all investigated reactions except for $^{40}\text{Ar} + ^{197}\text{Au}$; here the threshold was higher by about two units of Z and the overall efficiency was accordingly lower. The efficiency of $\cong 2\%$ for helium ions caused a small light-particle contamination which had to be corrected for.

In the following, M'_{IMF} denotes the associated IMF multiplicity, i.e., the number of IMF's accompanying the trigger particle or fragment, whereas M_{IMF} is the total IMF multiplicity for the selected class of events ($M_{\text{IMF}} = M'_{\text{IMF}} + 1$ for IMF triggered events). As an example, the observed distribution of M'_{IMF} for triggering fragments of $Z \geq 6$ from the reaction ^{18}O on ^{197}Au at $E/A = 84 \text{ MeV}$ is given in Fig. 1. In this case, in about 20% of all events, a second ($M'_{\text{IMF}} = 1$) or more ($M'_{\text{IMF}} > 1$) IMF's were detected with the PPAC array. This number was found to increase with increasing Z of the triggering particle and to saturate at $Z \geq 6$. Therefore, a trigger threshold of $Z \geq 6$ was applied to the data shown below.

In order to account for the PPAC efficiency gaps in the solid angle and in the element range $Z \leq 5$, and in order

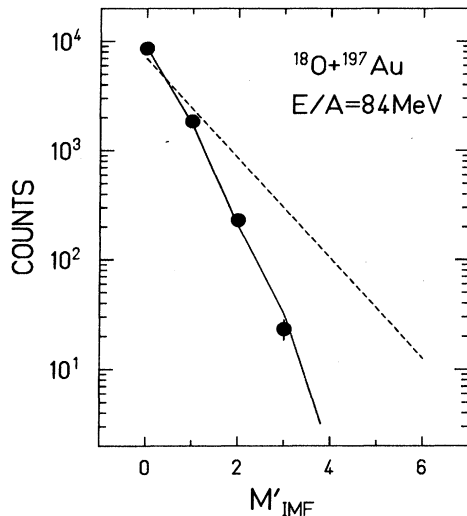


FIG. 1. Relative probability to detect M'_{IMF} fragments with the set of large area parallel plate detectors in coincidence with a fragment of $Z \geq 6$ for the reaction ^{18}O on ^{197}Au at $E/A = 84$ MeV (circles). The fit curve (solid line) was obtained by assuming an exponential form for the true multiplicity distribution (dashed line) and by applying a Monte Carlo model to account for the efficiency gap in solid angle and in the element range $Z \leq 5$.

to reconstruct the true fragment multiplicities M_{IMF} , a Monte Carlo model was developed. It is based on a moving-source parametrization of the inclusive IMF data measured with the telescope array (see Ref. 13 for details). Possible correlations of the energy spectra and angular distributions with the fragment multiplicity are thus neglected but this was found appropriate whenever the multiplicity dependence could be tested (similar observations were made by other groups^{6,7}). For the multiplicity distributions, an exponential form was assumed since it provided the best fits to the data (Fig. 1). The deduced mean values $\langle M_{IMF} \rangle$ of the true IMF multiplicity are 1.5 for the ^{18}O on ^{197}Au reaction (cf. Fig. 1) and, generally, in the range ≤ 1.6 for all investigated reactions. These values are small compared to the IMF multiplicities expected for a complete multifragmentation of the whole system^{1,2} and thus indicate that the reactions studied here may cover the threshold region to multifragment decay.

The following analysis, intended to determine the excitation energy of the composite system, rests on the assumption that preequilibrium light particles (PELP's, mass number $A \leq 4$) are emitted prior to the IMF's. This is experimentally supported by the observed difference in the degree of N/Z equilibration reached at the times of PELP and IMF emission¹¹ and by the different dynamical behavior of the two types of products.¹³ It has also been shown that the difference of time scales still holds for the case of multifragment emission in this class of reactions.¹⁰ As a consequence, the excitation energy E_x residing in the composite residual system at the time of IMF emission is essentially given by the difference of the collision energy $E_{c.m.}$ and the energy carried away by the PELP's includ-

ing their separation energies. In the laboratory system, which was chosen for convenience, the kinetic energy E_{recoil} of the heavy recoil nucleus also has to be considered in the energy balance:

$$E_x = E_{lab} - E_{PELP} - E_{recoil}.$$

A projectile source was not included since it was found that the requirement of an IMF at large angles selects central collisions with negligible amounts of energy and momentum remaining in projectile fragments.¹³

In order to determine E_{PELP} a Monte Carlo model of the PELP emission was constructed and fitted to the measured data. The angular and mass distributions were determined from moving-source fits to the inclusive cross sections as measured with the telescope array. Two sources, a target-velocity and an intermediate-velocity source of approximately half the beam velocity, were considered for each species, and the intermediate-velocity sources were associated with PELP emission. The parameters of the multiplicity distributions were determined from fits to the multiplicities of charged particles observed, in coincidence with IMF's, with the array of ten plastic detectors. The number of neutrons was assumed as N/Z times the number of protons where N and Z are the neutron and proton numbers of the emitting source containing equal numbers of nucleons from the projectile and from the target.^{11,14} The neutron source was assumed to have the same source characteristics as the proton source except for the missing Coulomb repulsion. The kinetic energies carried away by PELP's were then obtained by integrating the respective source intensities over energy and solid angle. Together with the separation energies they represent fractions between 0.35 and 0.70 of the total center-of-mass energies. The errors due to the uncertainty of the procedure were estimated as $\cong 20\%$ of E_{PELP} . The Monte Carlo results were also used to determine the masses and the kinetic energies ($10 \text{ MeV} \leq E_{recoil} \leq 100 \text{ MeV}$) of the recoiling composite nuclei.

The obtained mean excitation energies $\langle E_x \rangle$ are between 300 and 650 MeV for both targets. For a given projectile they increase with bombarding energy and for a given bombarding energy they increase with the projectile mass. For the studied reactions, $\langle E_x \rangle$ increases monotonically with the total projectile momentum but not with the total projectile energy. Figure 2 displays, as a function of $\langle E_x \rangle$, the summed cross sections for IMF production ($Z \geq 3$), the power-law exponents τ of fits to the inclusive element distributions according to $\sigma(Z) \propto Z^{-\tau}$, and the mean multiplicities $\langle M_{IMF} \rangle$ for the reactions on ^{197}Au . All three quantities, which may be considered the main observables characterizing IMF emission, are monotonically correlated with $\langle E_x \rangle$. In particular, the production cross section rises dramatically with increasing $\langle E_x \rangle$, reaching a value of $\sigma_{IMF} = 1.7b$ for ^{40}Ar at $E/A = 30$ MeV. The power-law parameter τ decreases with increasing $\langle E_x \rangle$ which expresses the increasing probability for the emission of larger fragments, and the mean IMF multiplicity increases slowly with $\langle E_x \rangle$.

The threshold energy of multifragment emission is an important quantity in statistical and dynamical models.^{1,15} In the studied class of reactions it is located near

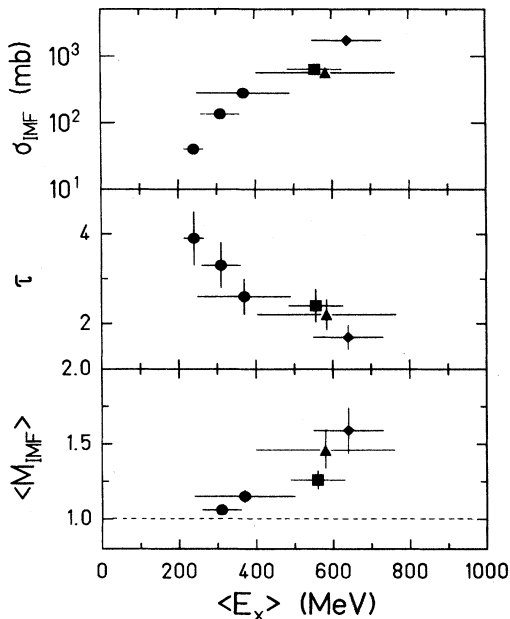


FIG. 2. The production cross section of intermediate mass fragments (top), the power-law exponent τ describing their inclusive element distribution (middle), and the mean multiplicity of intermediate mass fragments in collisions selected by the observation of one fragment of $Z \geq 6$ (bottom) as a function of the mean excitation energy deposited in the composite system for the reactions on ^{197}Au . The symbols denote the projectiles ^{12}C (circles), ^{20}Ne (squares), ^{18}O (triangles), and ^{40}Ar (diamonds). The multiplicity was not determined for ^{12}C of $E/A = 30$ MeV.

$\langle E_x \rangle \cong 300$ MeV where $\langle M_{\text{IMF}} \rangle$ starts to deviate from one, i.e., from the value characterizing binary disintegrations. There is no apparent difference in this respect between the reactions on the $^{\text{nat}}\text{Ag}$ and the ^{197}Au targets (Fig. 3). Reported preferences for binary disintegrations of $A \cong 150$ nuclei with $E_x \cong 280$ MeV (Ref. 16) and for multifragment decays of nuclei with $E_x \cong 800$ MeV (Ref. 8) are consistent with this threshold.

The systematic behavior of σ_{IMF} , τ , and $\langle M_{\text{IMF}} \rangle$ reveals the outstanding role played by the excitation energy $\langle E_x \rangle$ in the multifragment processes. Since this justifies statistical approaches to the problem we have performed calculations with the codes of Bondorf *et al.*¹ representing a statistical multifragmentation model, and of Charity *et al.*¹⁷ which treats sequential fragment emission within a Hauser-Feshbach formalism based on a transition state model.¹⁸ Both codes were modified in order to simulate the trigger conditions used in the experiment. The Hauser-Feshbach calculations were performed for initial orbital angular momenta $l=0\hbar$ and $l=50\hbar$ but the differences of the results were not significant. Figure 3 shows the fragment multiplicities calculated for nuclei with masses $A=100$ and 190 which were taken as representative for the reactions on $^{\text{nat}}\text{Ag}$ and ^{197}Au , respectively.

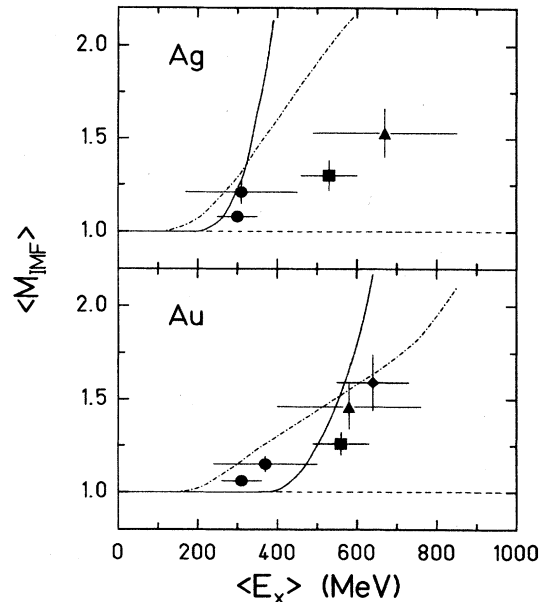


FIG. 3. Mean multiplicity of intermediate mass fragments [same quantity as in Fig. 2 (bottom)] as a function of the mean excitation energy deposited in the composite system for the reactions on silver (top) and gold targets (bottom). The symbols are chosen as in Fig. 2. The solid line gives the predictions of the statistical multifragmentation model of Bondorf *et al.* (Ref. 1) and the dash-dotted lines those of the Hauser-Feshbach code of Charity *et al.* (Ref. 17).

The observed onset of multifragment production is fairly well reproduced by both types of calculations. In particular, after smoothing over a finite range of excitation energies which might be required for a somewhat more realistic comparison to the data, the two predictions will be quite similar in the threshold region. At the higher excitation energies, however, the smaller multiplicities expected for sequential emission are closer to the data. If these differences in the predicted trends will be corroborated by further theoretical work, a distinction between the two qualitatively different reaction modes may be achieved by comparing to systematic data sets of the kind reported here.

The most significant difference between the data and the theory consists in their different mass dependences. The comparison of the multiplicities measured with the $^{\text{nat}}\text{Ag}$ and the ^{197}Au targets of rather different mass shows that the total amount of deposited energy E_x seems to be more important than the energy per nucleon E_x/A , which is the governing parameter in the statistical models. This may indicate that the breakup channels are selected before the entire system is thermalized and thus relate to the temporal evolution of the process. More generally, it may reflect the limitations of purely statistical descriptions which disregard the roles of the initial conditions as, e.g., the amount of compression reached in the primary reaction stage and of the dynamics of the evolution towards the breakup state (see, e.g., Refs. 19–21).

We are highly indebted to the staff of the CERN synchrotron and of the SARA facility for providing us with excellent heavy ion beams and W. Quick for invaluable contributions to the preparation of the experimental setup. We would like to thank Dr. H. Barz, Dr. H. Schulz, and Dr. R. Charity for making their codes available to us and for stimulating discussions.

*Present address: Lawrence Berkeley Laboratory, Berkeley, CA 94720.

†Present address: Texas A&M University, College Station, TX 77843.

¹J. Bondorf, R. Donangelo, I. N. Mishustin, and H. Schulz, Nucl Phys. **A444**, 460 (1985).

²D. H. E. Gross, Zhang Xiao-ze, and Xu Shu-yan, Phys. Rev. Lett. **56**, 1544 (1986).

³B. Jakobsson, G. Jönsson, B. Lindkvist, and A. Oskarsson, Z. Phys. A **307**, 293 (1982).

⁴E. M. Friedlander, H. H. Heckman, and Y. J. Karant, Phys. Rev. C **27**, 2436 (1983).

⁵C. J. Waddington and P. S. Freier, Phys. Rev. C **31**, 888 (1985).

⁶A. I. Warwick *et al.*, Phys. Rev. C **27**, 1083 (1983).

⁷D. J. Fields *et al.*, Phys. Rev. C **34**, 536 (1986).

⁸G. Klotz-Engmann *et al.*, Phys. Lett. B **187**, 245 (1987).

⁹K. G. R. Doss *et al.*, Phys. Rev. Lett. **59**, 2720 (1987).

¹⁰R. Trockel *et al.*, Phys. Rev. Lett. **59**, 2844 (1987).

¹¹R. Wada *et al.*, Phys. Rev. Lett. **58**, 1829 (1987).

¹²H. J. Rabe *et al.*, Phys. Lett. B **196**, 439 (1987).

¹³R. Trockel, Ph.D. thesis, Universität Heidelberg, Report No. GSI-87-17, 1987 (unpublished).

¹⁴C. K. Gelbke, Nucl. Phys. **A400**, 473c (1983).

¹⁵G. F. Bertsch and P. J. Siemens, Phys. Lett. B **126**, 9 (1983).

¹⁶D. R. Bowman *et al.*, Phys. Lett. B **189**, 282 (1987).

¹⁷R. J. Charity *et al.*, Nucl. Phys. **A483**, 371 (1988).

¹⁸L. G. Moretto, Nucl. Phys. **A247**, 211 (1975).

¹⁹J. Nemeth, M. Barranco, J. Desbois, and C. Ngô, Z. Phys. **A325**, 347 (1986).

²⁰H. Heiselberg, C. J. Pethick, and D. G. Ravenhall, Phys. Rev. Lett. **61**, 818 (1988).

²¹K. Sneppen, D. Cussol, and C. Gregoire (unpublished).